



The Impact of Psyllium Husk Addition on the Some Physical Properties of PEO Polymer

Alhak A. M. Hassan^{*}, Abdulazeez O. Mousa Al-Ogaili[†]

Department of Physics, College of Science, University of Babylon, Babylon 51001, Iraq

Corresponding Author Email: sci.elhaq.abd@uobabylon.edu.iq



Copyright: ©2025 The authors. This article is published by IIETA and is licensed under the CC BY 4.0 license (<http://creativecommons.org/licenses/by/4.0/>).

<https://doi.org/10.18280/rcma.350109>

ABSTRACT

Received: 16 January 2025
Revised: 14 February 2025
Accepted: 21 February 2025
Available online: 28 February 2025

Keywords:

PEO, psyllium husk, XRD, FTIR, UV/Vis optical absorption

This research included the effect of psyllium (*Plantago ovata*) husk powder (5 wt.% PHP) on the structural and optical properties of a composite consisting of ultra-high molecular weight polyethylene oxide (PEO). The composite films of PEO and PEO/Psyllium husk were prepared by the solution casting method. XRD revealed the semicrystalline nature of all as-prepared films. FTIR analysis revealed that PEO possesses several types of functional groups and conjugated dual bonds, which include C-H stretching, bending vibrations, and O-H bonds and appeared to have C-O-C triplet bond. According to FESEM's analysis of the films' morphology, psyllium husks exhibit a needle-like shape. In EDX, the elemental composition of PEO film revealed the existence of C and O elements at the amounts of 54.6% and 45.4%, but upon doping with C, O, Al, Si, Ni, and Zn. The optical properties of the films with thicknesses of 97.5 and 97 μm were determined using transmittance, reflectance, Tauc plot, reflective index, and extinction coefficient. The absorbance curve of PEO film showed one absorption peak located at 240 nm. The bandgaps of the direct and indirect transitions were decreased from 4.5 eV to 3.4 eV and 3.3 eV to 1.5 eV, respectively.

1. INTRODUCTION

Bionanotechnology is a scientific and technological breakthrough that has provided solutions in practically every field. However, developing environmentally friendly and inexpensive biomaterials remains a major issue. The demand to synthesize green and nature friendly materials derived from biological resources and waste materials has grown exponentially [1]. A promising study opportunity emerged from the necessity to reduce waste and develop sustainable solutions through the use of newly developed resources that are renewable. This opportunity demonstrated the comparative benefits of utilizing diverse oriented waste biomass as renewable, economical, and widespread supplies for decreasing energy and feedstock costs [2]. Managing the vast quantities of waste in human environments and natural ecosystems is challenging. The management of waste is a substantial challenge for humanity, and it will persist as the population expands at a rapid pace and natural resources diminish [2]. Poly (ethylene oxide) (PEO) is a polyether compound that has a chemical structure of $\text{H}-(\text{O}-\text{CH}_2-\text{CH}_2)_n-\text{OH}$. PEO is also referred to as polyethylene glycol (PEG) based on its molecular weight. Typically, PEO is a polymer with a molecular weight over 20,000 g/mol, whereas PEG denotes the oligomer of ethylene oxide or the polymer with a molecular weight less than 20,000 g/mol. PEO is typically synthesized through cationic or anionic ring-opening polymerization of ethylene oxide, contingent upon the catalyst employed. PEO is a widely accessible product with numerous

applications. PEO exhibits low toxicity, making it suitable for diverse applications, including medical, chemical, biological, commercial, and industrial sectors [3]. PEO is a non-ionic, hydrophilic, water-soluble, semi-crystalline polymer that's commonly utilized to deliver drugs, scaffold fabrication, and tissue engineering. To satisfy the requirements of any application, PEO must possess suitable thermodynamic characteristics, crystallization kinetics, and an adequate molecular weight (Mw) [4]. Psyllium seed husk (PSH) is a gelatinous, water-soluble mucilage that is taken from *Plantago ovata* [5]. The psyllium husk is the seed's mucilaginous outer layer. The plant's primary component that is utilized in the production of psyllium products and possesses nutritional value is this. Polysaccharides, glycosides, choline, vitamin B1, and proteins comprise this material. It includes a high fiber content primarily consisting of hemicellulose. Hemicellulose is a complex polysaccharide that exists in cereals, vegetables, and fruits. Although indigestible, it is partially fermented in the colon, providing nourishment to intestinal flora. The outer layer of seeds is removed to obtain psyllium husk. It has around 70% soluble fiber and 30% insoluble fiber. Husk is a white fibrous material utilized in different sectors, including pharmaceuticals, cosmetics, and food manufacturing. Different grades of psyllium husk are accessible, differentiated by purity and mesh size to meet user requirements. Psyllium husk serves as the primary material for the production of psyllium mucilage. Alcohol is used in an aqueous solution to precipitate it. subsequently washed with acetone, and finally dried. Psyllium husk powder is produced from the husk

through grinding with varying particle mesh sizes [6]. Psyllium husk powder (PHP) is a natural dietary fiber recognized for its substantial water-soluble fiber content and it served as a prebiotic [7]. A conventional plant called "ISABGOL" is used as a home remedy for many different diseases in all cultures. These include chronic constipation, diarrhea, inflammation of the GI and genitourinary tract mucous membranes, duodenal ulcers, gonorrhoea, piles, etc. It can be used as a bulk-forming, non-irritating laxative drug, demulcent, cervical dilator, etc. Drugs are nearly always supplied as drug delivery systems (DDSs), rather than as pure chemical compounds [8]. Psyllium husk (PH) is utilized as a water-soluble, gel-reducing substance and is frequently employed in Asian nations as a natural remedy for metabolic diseases, hypertension, and hypercholesterolemia [9]. In 2023, AL-Akhras et al. [10] investigated PEO thin films containing curcumin nanoparticles optically and chemically. The findings show that the UV-Vis data's refractive index ranges from 1.5 to 2. While curcumin NPs and PEO-Curcumin nanocomposite thin films had bandgap energies of 2.49 eV and 4.16 eV, respectively, the PEO thin film has a bandgap energy of 4.16 eV. According to the findings, the optical absorption coefficient rises as the layer thickness decreases. Telfah et al. [11] investigated the structural, optical, and electrical properties of films containing polyethylene oxide and fullerene nanocomposite. The findings show that adding C60 to PEO sheets increases the composite's electrical conductivity and enhances its ability to absorb UV radiation. Abdali et al. [12] showed that *Elettaria cardamomum* husk ash may be used as feedstock nanofibers to enhance the structural, optical, dielectric, and antibacterial properties of PEO polymer for use in biological and optoelectronic applications. The results show the bandgaps for the direct and indirect transitions were lowered from 5.85 eV to 2.85 eV and 3.85 eV to 2.25 eV, respectively. The main aim of this study is to investigate the impact of psyllium husk ash nanofibers on the structural and optical properties of PEO polymer to make it appropriate for various optoelectronic devices, UV sunscreens, organic solar cells, and food packaging applications.

2. MATERIALS

The polymer used (PEO) is white, granular and water-soluble, with a molecular weight of (3×10^6 g/mol.) and high purity (98%), it was manufactured by a company (Cheng Du Micxy Chemical Co., Ltd.), and psyllium husk was purchased from a local supermarket in Iraq.

3. THE PREPARATION OF PHP NANOFIBERS

The PHP was prepared from *Ispaghula* plant husks collected and cleaned several times to remove all dust pollutants and impurities, where husks are only used as a filler material. The obtained extract was ground using the powder grinder approach for 60 min and for intermittent periods. This is the powder grinder; it has a distinctive characteristic: universal mill, stainless steel housing, 50-60 Hz, fineness 30-300 M, RPM 25000 r/min., and 650 W. After that, 0.05 g of the ground PHP nanofibers was used. The PHP extract is then utilized as a sustainable filler in each step of the present work.

4. NANOCOMPOSITE FILMS PREPARATION

At the onset, 1 g of PEO was separately dissolved in deionized water (H_2O) using a Stuart magnetic stirrer at room temperature ($20 \pm 5^\circ C$) for 1 h until getting a fully homogenous solution. Then, the polymer solution was cast in the 5 cm plastic Petri dish and left to dry for 10 days under the chemical hood to avoid dust pollution at room temperature (RT), resulting in a pristine PEO polymer film. In the loading processes, a certain weight ratio of PHP nanofibers (5 wt.%) was independently embedded into PEO and stirred for 40 min, and the exact first procedure of preparation was applied. The thicknesses of the P-PHP nanocomposite films were computed by using a thickness measuring device (Micro Printer), ranging from 97.5 to 97 μm . Finally, the samples were encoded as PEO and P-5PHP.

5. INSTRUMENTATIONS

The grinding process was done using a powder grinder supplied by the company (Cheng Du Micxy Chemical Co., Ltd.). The XRD analysis was examined by using Aeris-Malvern Panalytical's instrument [wavelength = 1.54 Å, settings of generator = 40 kV and 30 mA, step size (2-Theta = $0.05^\circ/1.0$ s), and 2-Theta range between 10° and 80°]. FTIR spectra was recorded by using an FTIR type Vertex 70, Bruker, Germany. The FESEM and EDX were investigated by Alkora Company Sem Lab, Baghdad, Iraq, INSPECT F 50 FESEM. The optical properties were studied by using a Shimadzu spectrometer.

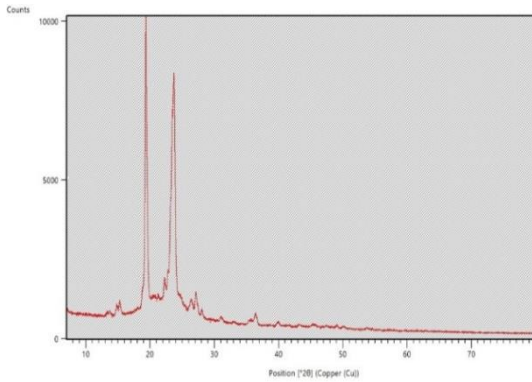
6. RESULTS AND DISCUSSION

6.1 XRD analysis

Figure 1 illustrates the XRD spectra for PEO and PEO/PHP nanocomposite. In Figure 1(a), pure PEO displays a significant intensity peak at 19.4° and the other considerable maximum at 23.5° , illustrating high-intensity diffraction peaks, along with minor peaks at elevated angles of $2\theta = 27.10^\circ$, 36.39° , and 39.89° , thereby exhibiting the semicrystalline characteristics of PEO.

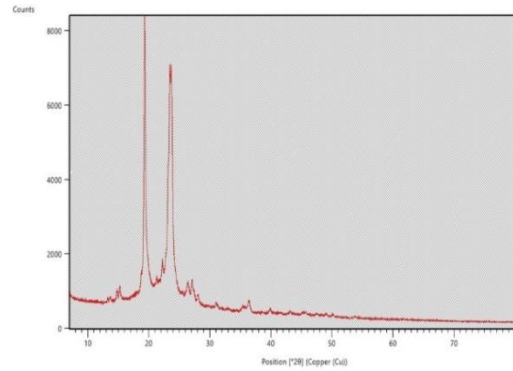
The three peaks are interconnected by the (112, 120 and 121) planes [13, 14]. The tendency of the PEO polymer peaks to broaden indicates that the obtained PEO has a linear and semicrystalline structure. The unit's responsibility was to stabilize the PEO chemically and electrochemically [12]. Generally, as a polymer undergoes crystallization, organized structures develop hierarchically across multiple length scales. The Deformation of a polymer chain generally results in the formation of a folded-chain lamellar crystal, characterized by a unique molecular periodicity. This folded arrangement expands unrestrained in two lateral directions. Nonetheless, the extension of the chain is constrained, with a majority of defects occurring at the folding interfaces. The peaks shown in Figure 1 are the result of strong intermolecular interactions between PEO chains linked by hydrogen bonds and the arrangement of the polyether side chains. The outcome obtained aligns with previous studies findings by Abdali et al. [12-14]. This indicates that the crystalline peaks in a pure PEO specimen are observed at these particular angles. The distinct diffraction peak reflects the crystalline or semicrystalline

nature of the PEO polymer surface [11]. Figure 1(b) shows the XRD pattern of the PEO/PHP composite. The XRD spectrum reveals the semicrystalline nature of the composite, exhibiting two significant peaks at 19.3° and 23.6°, which are associated with the semicrystalline structure of the PEO polymer. The



(a) XRD analyses of pure PEO

XRD spectrum of the composite sample displays several low-intensity peaks at $2\theta = 26.3^\circ, 27.1^\circ, 36.3^\circ,$ and 39.8° . The most significant diffraction peaks of nanocomposite films exhibit a decrease in intensity accompanied by an increase in width [10].



(b) XRD analyses of PEO/PHP nanocomposite

Figure 1. XRD analyses of (a) pure PEO and (b) PEO/PHP nanocomposite

The crystallite size (D) is determined by the Debye-Scherrer equation, as stated in Eq. (1) [12].

$$D = K\lambda/\beta\cos\theta \quad (1)$$

where, $k = 0.9$ and β are the full width at half maximum (FWHM), the D varies as $(1/\cos \Theta)$, and the lattice strain values vary as (\tan) from the FWHM. D of the samples was impacted and raised from 39.6 nm to 46.5 nm upon PHP nanofibers loaded into PEO polymer. In conclusion, it is noted that raising the doping ratio of PHP nanofibers broadened the peaks of diffraction of the host PEO, which may be credited to the variance in the deacetylation degree of the host PEO. The peak intensities were notably decreased; this inculcated a variation in PEO polymer's crystalline size, where PEO's crystallite size increased upon PHP nanofiber loading [15]. There are no new peaks discernible in the XRD patterns of the nanocomposite films.

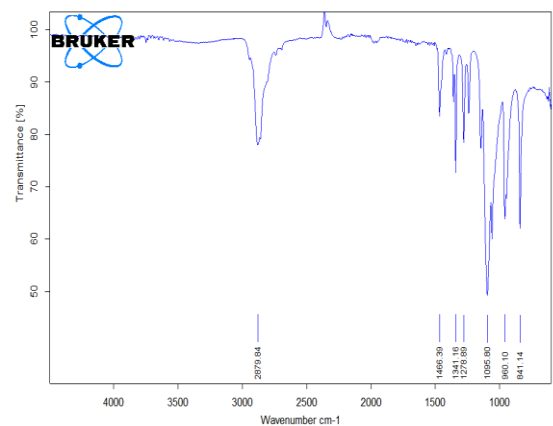
6.2 FTIR analysis

FTIR was employed for identifying and describing the functional categories of the PEO and PEO/PHP nanocomposite film. The functional groups of the PEO and PEO/PHP samples can be acquired by examining the spectrum region of 400 to 4000 cm^{-1} , as this range facilitates the detection of the frequencies of vibration of the chemical bonds constituting both organic and inorganic molecules. Vibrations within a specific frequency range cause absorption at functional groups, which has a distinct characteristic of infrared absorption [14]. Figure 2(a) illustrates the FTIR spectra of PEO and PEO/PHP. The PEO spectrum exhibited a spectral band at 2883 cm^{-1} corresponding to C-H stretching vibrations and at 1467 and 1341 cm^{-1} for C-H bend vibrations. The absorption bands between 1280 and 1100 cm^{-1} resulted from the stretching vibrations of the alcoholic O-H and C-O-C ether bonds [16-18]. 1095 cm^{-1} is known as the triplet, which refers to the symmetrical stretching of the C-O-C group, signifying the presence of a crystalline phase of PEO [15]. CH_2 rocking and C-O-C vibration mode at 960 cm^{-1} , CH_2 rocking at 841 cm^{-1} [16]. Furthermore, the band at 840 cm^{-1} represents the stretching vibration of the C-O-C and C-C

molecular bonds [19]. These findings indicate the presence of high crystallinity inside the PEO structure [20]. Figure 2(b) displays the FTIR spectra of PEO/PHP. There are no new peaks, where the observed shifts in these bands compared to those for pure PEO indicate a physical interaction between the polymer matrix and PHP, predicted due to intermolecular hydrogen bonding [19]. Table 1 presents the band assignments for FTIR characterization of PEO and PEO/PHP.



(a) FTIR spectra of PEO



(b) FTIR spectra of PEO/PHP nanocomposite

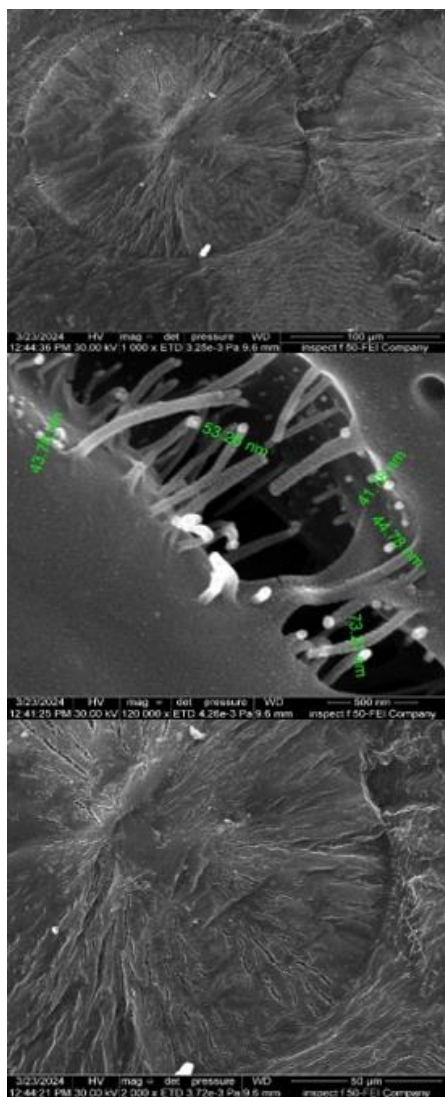
Figure 2. FTIR spectra of (a) PEO, (b) PEO/PHP nanocomposite

Table 1. The band assignments for FTIR characterization of PEO and PEO/ PHP [16, 17]

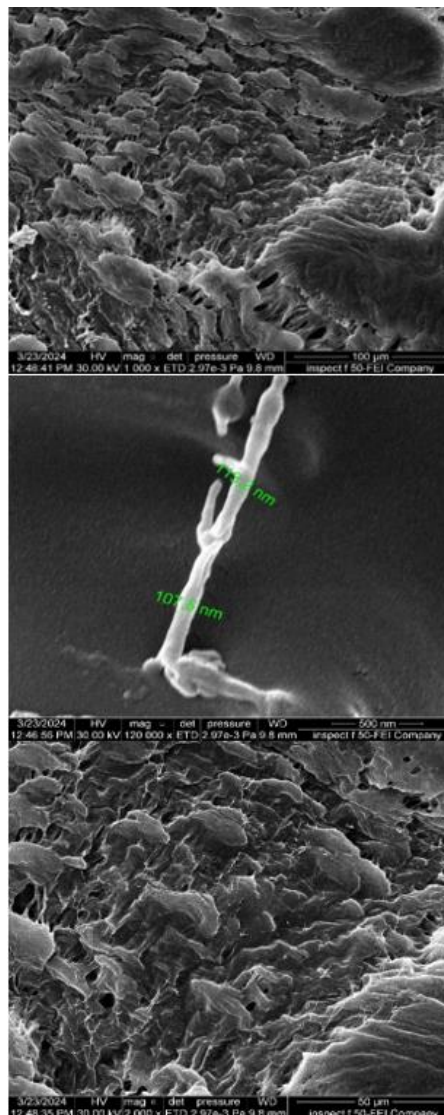
Absorption (cm ⁻¹)	Appearance	Group	Compound Class
2878	medium	C-H stretching	alkane
1466	medium	C-H bending	alkane
1341	medium	C-H bending	alkane
1278	strong	C-O stretching	Alkyl aryl ether
1095	strong	C-O stretching	Secondary alcohol
960	strong	C=C bending	alkene
841	medium	C=C bending	alkene

6.3 The morphological study

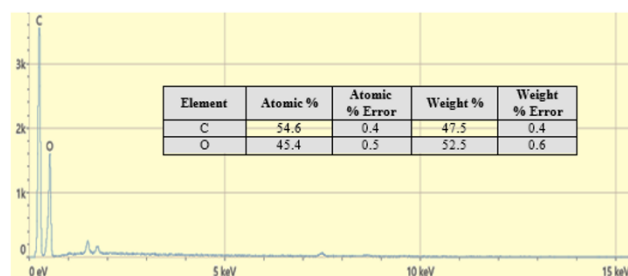
Field Emission Scanning Electron Microscopy is a type of high-resolution microscope that uses the principle of electrons to create high-resolution, three-dimensional content images of the resulting film's surfaces. an FESEM uses a field emission source to produce a much finer electron beam [21]. FESEM is commonly used in nanotechnology, materials science, and other sectors where high-resolution surface imaging and analysis is critical [22]. The morphologies of the PEO and P-PHP films were rigorously surveyed, examined, and studied Figure 3.



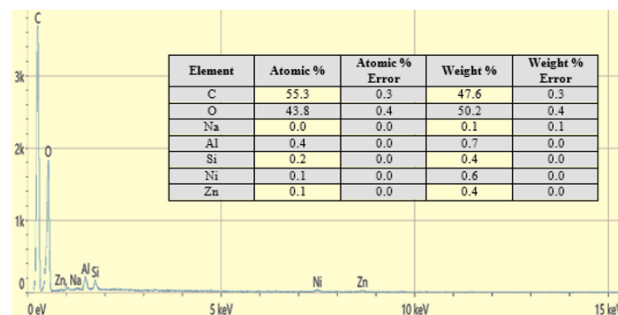
(a) FESEM of the resultant film of PEO



(b) FESEM of the resultant film of PEO/PHP nanocomposite



(c) EDX of PEO film



(d) EDX of PEO/PHP films

Figure 3. FESEM-EDX of the resultant film: (a) PEO, (b) PEO/PHP nanocomposite, (c) EDX of PEO film, and (d) EDX of PEO/PHP films

The FESEM micrographs of the pure PEO Figure 3(a) display the rough morphology with some smoother surface due to its semi-crystalline nature. It is clear from Figure 3(b) that there was no aggregation or cracking in the resulting films between these input materials. Where needle-like shapes appeared as a result of psyllium husk nanoparticles, which led to basic formations such as bimetallic nanoparticles. The psyllium husk additions were fine and homogeneously distributed within the PEO matrix, and this is probably due to the ability of this polymer to integrate with the particles of the nanocomposite [23, 24]. The results of the images showed that the grain size was 53.26 nm. The technique was also used in Energy Dispersive X-ray Spectroscopy (EDX). An analytical approach employed to examine components in order to ascertain the chemical characteristics of samples, categorized as a form of X-ray spectroscopy. In this technique, both oxygen and carbon appeared to represent the polymer. The elemental composition of PEO film Figure 3(c) revealed the existence of C and O elements at the amounts of 54.6% and 45.4%. Still, the EDX of P-PHP films Figure 3(d) verified the existence of C, O, Al, Si, Ni, and Zn elements at the amounts of 55.3, 43.8, 0.4, 0.2, 0.1, and 0.1 wt.%, respectively. It is noted from these figures that the high-intensity element is C due to the polymer structure. This technique, both oxygen and carbon appeared to represent the polymer. The elemental composition of PEO film Figure 3(c) revealed the existence of C and O elements at the amounts of 54.6% and 45.4%. Still, the EDX of P-PHP films Figure 3(d) verified the existence of C, O, Al, Si, Ni, and Zn elements at the amounts of 55.3, 43.8, 0.4, 0.2, 0.1, and 0.1 wt.%, respectively. It is noted from these figures that the high-intensity element is C due to the polymer structure.

6.4 Ultraviolet and visible analysis UV/Vis

A double-beam, shemadzo 1800 spectrophotometer, in the optical range between 190-1100 nm was utilized to record the UV-V spectrum. UV/Vis analysis involves quantifying the extent of light beam attenuation subsequent to its passage through a sample or reflection from the surface of a sample. The ultraviolet and visible absorption spectra of the PEO and PEO/PHP nanocomposite are illustrated in Figure 4, the pure absorption spectrum exhibits a peak at 240 nm, probably ascribed to $n \rightarrow \pi^*$ transitions (R-band) due to the presence of a single bond; thus, it is presumed to absorb photons only in the far UV area. When psyllium husks are added to the polymeric matrix of PEO, the absorbance goes up a lot in the UV/Vis range. This is shown by the sample having a higher absorption coefficient and its absorption edge moving toward longer wavelengths. The red shift of the absorption edge in the doped PEO/PHP represents the complexation between PHP and the polymer. Furthermore, it indicates the alteration in the optical energy gap, which occurs due to the variation in crystallinity within the polymer matrix [25]. In P-PHP film, the noticed shifting of the maximum absorption towards higher wavelengths at the absorption edge next the lower band gap confirms that the PHP nanofiber grains exhibit a variety of shapes and sizes across the film surface, as verified by FESEM analysis [12]. Transmittance and reflectance spectra have been employed to investigate all-optical characteristics to derive the pertinent variables for optical electronics applications, as illustrated in Figure 5. Transmittance values were similar across PEO and PEO-psyllium husks, with a cut-off below 440 nm, but the PEO membrane exhibited a

transmittance cut-off beginning below 360 nm [10]. All samples' transmittance curves indicate a trend into saturation, with the polymer film achieving a maximum average transmittance of approximately 50% in the visible and NIR areas of the spectrum. Still, it declines with the rising loading ratio of PHP nanofibers in the PEO matrix. This characteristic was attributed to the film's morphology and the absorption properties. The low transmittance of P-PHP film in the UV spectrum renders it suitable for applications like solar collectors, UV shielding, and pharmaceutical packaging [12]. The absorption coefficient represents a fundamental optical property that can be ascertained through measurements of transmittance and reflectance. Understanding the optical absorption coefficient provides an additional method for analyzing the bandgap energy of nanocomposite films. Figure 6 displays the optical absorption coefficient (α) as a function of wavelength for nanocomposite films of PEO and PEO/PHP. The absorption coefficient is often quantified to indicate the probability of photon absorption per infinitesimal path length. The optical absorption coefficient is significantly influenced by film thickness and increases as film thickness decreases.

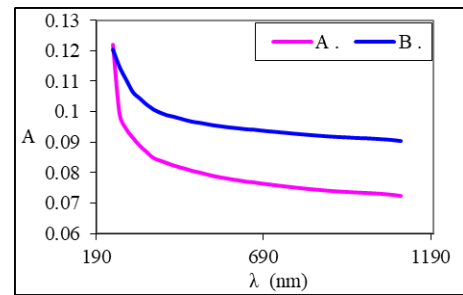
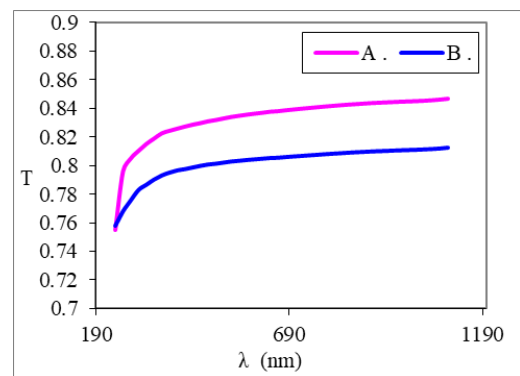
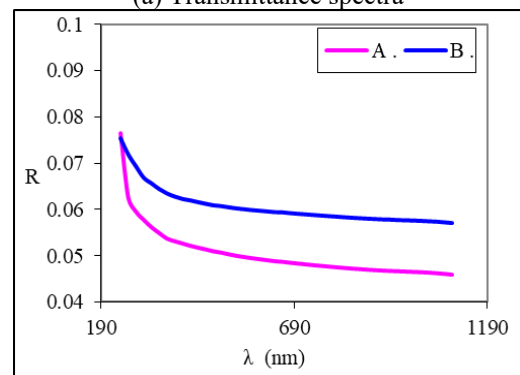


Figure 4. Absorbance spectra of (a) PEO and (b) PEO/PHP nanocomposite films



(a) Transmittance spectra



(b) Reflectance spectra

Figure 5. Transmittance and Reflectance spectra of PEO and PEO/PHP nanocomposite films

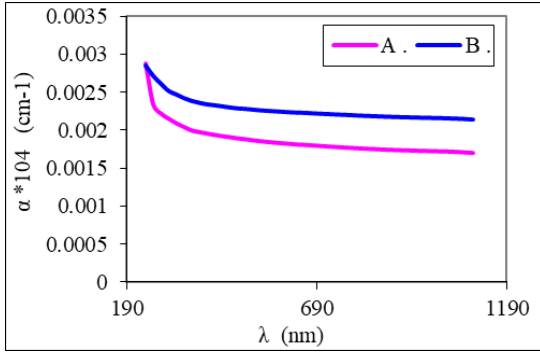


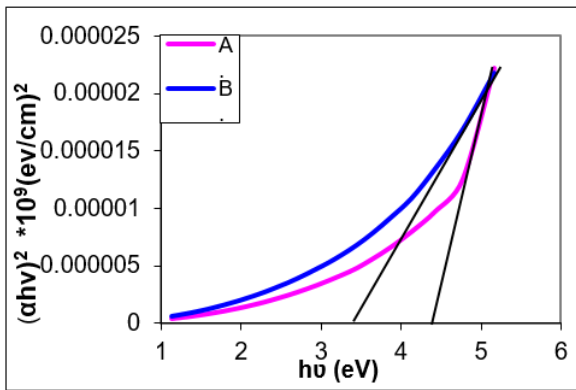
Figure 6. Spectra of the optical absorption coefficient (α) for nanocomposite films of PEO and PEO/PHP

In general, the relationship presented in Eq. (2) is utilized to derive the absorption coefficient (A) [12], which is considered a sensitive physical way to give us vital information about the sorts of charges transported in a band and around the value of the bandgap energy.

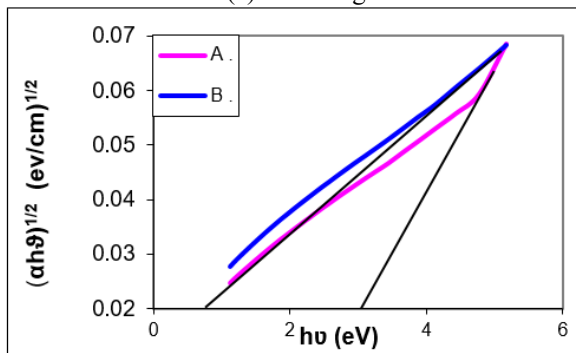
$$A = 2.303(a/t) \quad (2)$$

where, a is the absorbance, t is the film thickness. The coefficient of absorption value is a significant point in selecting the type of electron transition. The coefficient of absorption values less than 10^4 cm^{-1} refers to indirect electron transition and vice versa concerning $A > 10^4 \text{ cm}^{-1}$. The optical energy gap is related to the energy of the photon (E_{ph}) and the coefficient of absorption t in the Tauc plot as expressed in Eq. (3).

$$Ah\nu = B(h\nu - E_g^{opt} \pm E_{ph})^n \quad (3)$$



(a) Direct Eg



(b) Indirect Eg

Figure 7. Tauc optical bandgap energy of PEO and PEO/PHP nanocomposite films

where, B represents the disorder parameter for band tailing, whereas n denotes the type of optical transition of studied materials ($n = 0.5$ for indirect transitions and $n = 2$ for direct transitions). The direct and indirect optical band gap energy can be determined from the plot of $(\alpha h\nu)^{1/n}$ versus photon energy ($h\nu$) as illustrated in Figure 7. The obtained bandgaps were obtained by projecting the linear portion of the curve to the $h\nu$ axis. The formation of imperfections and disarrays in the materials, which are close to the conduction band, may explain why the optical energy gap has decreased with the increase of additives because of the generation of new energy states (localized states) in the band gap region, which is related to the interaction between host PEO and PHP nanofibers. As a result, it can soak up low-energy photons. In addition, the energy bandgap values show that the indirect transition's energy bandgap is smaller than the direct transition's. In direct transitions, the energy bandgap values decrease from (4.5 eV) in PEO to (3.4 eV) in PEO/PHP, while in indirect transitions, the energy bandgap values decrease from (3.3 eV) in PEO to (1.5 eV) in PEO/PHP, indicating that the transition between the top of the valence band (TVB) and the bottom of the conduction band (BCB) occurred via the indirect transition in the P-PHP system. These findings match the literature results [10, 12].

Investigating the behavior of refractive index is important for understanding many optical phenomena. The refractive index, n , is intricately connected to the electrical polarization of ions and the local field within of optical substances. This parameter is essential for integrated optical devices. The optical dielectric constant is considered as an essential attribute in the development of novel ingredients for a range of optical and electrical applications. Reflectance and absorption can be used to calculate a substance's refractive index when an electromagnetic light beam passes through it, as express in Eq. (4).

$$n^*(\lambda) = n(\lambda) + k(\lambda) \quad (4)$$

In this context, n^* denotes the complex refractive index, with n representing the real component associated with the actual velocity and (k) signifying the extinction coefficient. The Fresnel equation facilitates the determination of the refractive indices of both pure PEO films and PEO films doped with PHP, as given in Eq. (5), by utilizing the reflectance value (R) and the optical extinction coefficient.

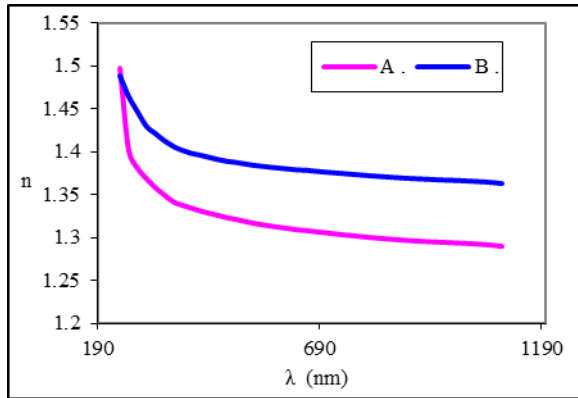
$$k = \alpha\lambda/4\pi \quad (5)$$

The absorption coefficient and the wavelength are given in Eq. (6).

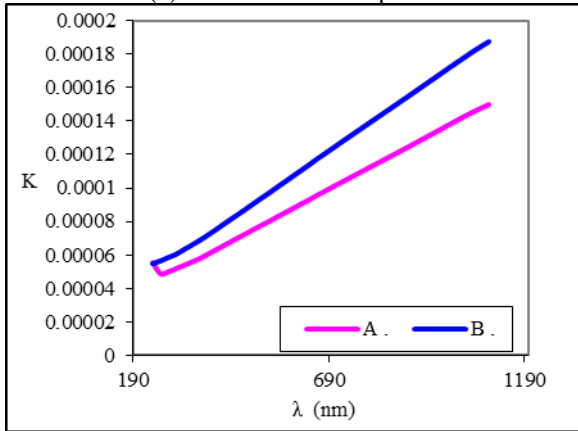
$$n(\lambda) = \sqrt{\frac{4R}{(1-R)^2} - K^2} + \frac{1+R}{1-R} \quad (6)$$

The refractive index, $n(\lambda)$, determines the transparency of materials as light beam passes through an optical medium. For materials that are fully transparent, $n(\lambda)$ is approaching zero, while positive values signify light absorption. Figure 8(a) illustrates the refractive index, $n(\lambda)$, for both pure PEO and PEO doped with PHP. The results indicated that adding psyllium husk to PEO polymer raised the refractive index from 1.28 to 1.37, which is probably related to the formation of space charge in the PHP [14]. The refractive index decreases

significantly in the visible spectrum as the wavelength increases [10]. This rise in refractive index extends the use and application of these materials in optoelectronics field. Figure 8(b) illustrates the variance of the extinction coefficient for PEO and PEO/PHP nanocomposite films as an indication of wavelength (λ), respectively. The figure illustrates the increase in the extinction coefficient of PEO/PHP nanocomposite films with the increasing in the wavelength of the incident light in the UV region, this is attributable to the high absorption in certain regions. Furthermore, the extinction coefficient increases in the visible and near-infrared spectra.



(a) Refractive index spectra



(b) Extinction coefficient spectra

Figure 8. (a) Refractive index spectra of PEO and its nanocomposites (b) Extinction coefficient spectra of PEO and PEO/PHP nanocomposite film

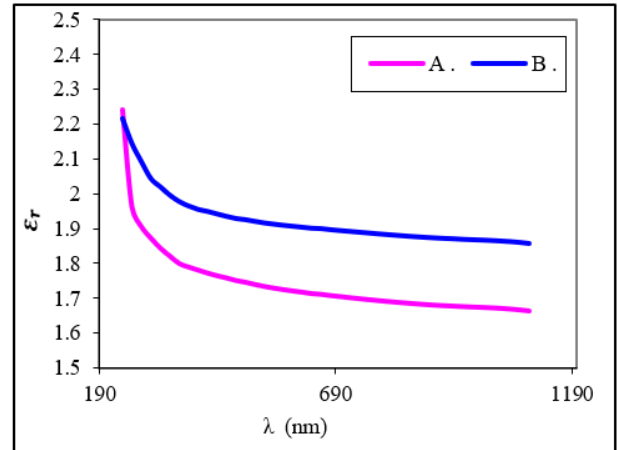
The real component of the dielectric constant indicates the extent to which the light speed is reduced in the samples, while the imaginary component illustrates the energy absorption characteristics of a dielectric in response to an electric field, attributed to the movement of the dipole [26]. The real and imaginary parts of the dielectric constant are measured using Eqs. (7) and (8) [27, 28].

$$\epsilon_r = n^2 - k^2 \quad (7)$$

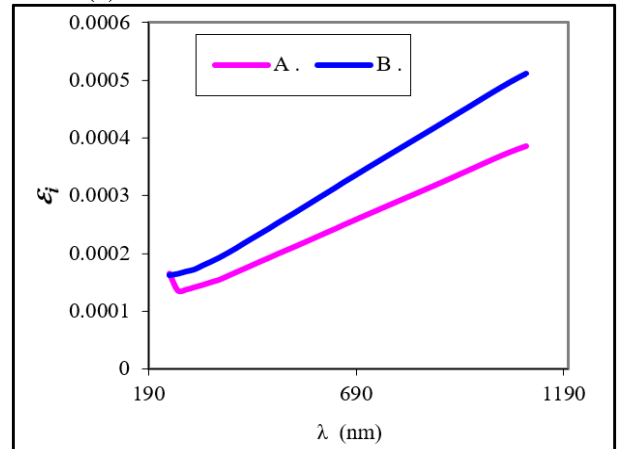
$$\epsilon_i = 2nk \quad (8)$$

Figure 9 displays the variation of the real part (ϵ_r) and imaginary part (ϵ_i) of the dielectric constant with the wavelength for (PHP) and (PEO/PHP) nanocomposites, respectively. The real component of the dielectric constant exhibits behavior like that of the refractive index (n), as the extinction coefficient (k^2) is significantly smaller than the

refractive index (n^2). Conversely, the imaginary component of the dielectric constant is fundamentally proportional to the values of the extinction coefficient (k) values [29]. The dielectric constant of PEO and their nanocomposites with PHP nanofibers increases; this is related to a reduction in the scattering of the photon that was incident. The imaginary part of the dielectric constant of nanocomposites is increased. This is due to an increase in the absorption coefficient of nanocomposites, and this behavior may be related to an increase in discharger alignments [30, 31].



(a) The behavior of real dielectric constant



(b) The behavior of imaginary dielectric constant

Figure 9. The behavior of (a) real dielectric constant and (b) imaginary dielectric constant against wavelength for of PEO and PEO/PHP nanocomposite films

7. CONCLUSIONS

In conclusion, PEO and P-PHP nanocomposite films were produced for the first time using the casting procedure. The XRD results indicate the semicrystalline nature of the composite, evidenced by two significant peaks at 19.3° and 23.6° , attributed to the semicrystalline polymer's existence. The main diffraction peaks of the nanocomposite films display a reduction in intensity and an increase in width. Also, it is noted that raising the doping ratio of PHP nanofibers broadened the peaks of diffraction of the host PEO, where PEO's crystallite size increased upon PHP nanofiber loading. The XRD patterns for the nanocomposite films exhibit no new peaks. An FTIR analysis revealed that PEO contains numerous functional groups and conjugate double bonds, that includes C-H stretching vibrations, C-H bending vibrations, and O-H

bonds, and appeared C-O-C triplet bonds. The FTIR spectra of PEO/PHP display that there are no new peaks; these bands were displaced relative to those seen for pure PEO, signifying a physical interaction between the polymer matrix and PHP. The FESEM image lineup of the PEO film manifested homogeneity and a defect-free surface, and there was no aggregation or cracking in the resulting films between these input materials. The psyllium husk additions were fine and homogeneously distributed within the PEO matrix, and this is probably due to the ability of this polymer to integrate with the particles of the nanocomposite. In EDX The elemental composition of PEO film revealed the existence of C and O elements at the amounts of 54.6% and 45.4%, but upon doping C, O, Al, Si, Ni, and Zn. It is noted that the high-intensity element is C due to the polymer structure. The optical coefficients were boosted after embedding; the spectrum of pure substances exhibits an absorption peak around 240 nm, likely due to $n \rightarrow \pi^*$ transitions (R-band) associated with the presence of single bonds; thus, it is presumed to absorb radiation exclusively in the far UV area. The addition of psyllium husks into the polymeric matrix of PEO leads to a significant increase in absorbance in the UV/Vis. The P-PHP film indicates a shift of maximum absorption to higher wavelengths at the absorption edge near the lower band gap signifies that the PHP nanofiber grains exhibit varied shapes and sizes across the film surface. All-optical properties were investigated using Transmittance and reflectance spectra to determine the pertinent parameters for optoelectronic applications. The PEO membrane has a transmittance cut-off start below 360 nm, while PEO and PEO-psyllium husks showed comparable transmittance values with a cut-off below 440 nm. PEO film's low transmittance in the UV region makes it suitable for applications like solar collectors, UV shielding, and containers for pharmaceutical storage. In direct transitions, the energy bandgap values decrease from (4.5 eV) in PEO to (3.4 eV) in PEO/PHP, while in indirect transitions, the energy bandgap values decrease from (3.3 eV) in PEO to (1.5 eV) in PEO/PHP. The results indicate that adding psyllium husk to PEO polymer raises the refractive index from 1.28 to around 1.37. The increase of the refractive index enhances the use of these materials in the optoelectronics field.

REFERENCES

- [1] Garg, V.K., Pandey, A., Kataria, N., Faggio, C. (Eds.). (2023). *Pharmaceuticals in Aquatic Environments: Remediation Technologies and Future Challenges* (1st ed.). CRC Press. <https://doi.org/10.1201/9781003436607>
- [2] Molahalli, V., Sharma, A., Bijapur, K., Soman, G., Chattham, N., Hegde, G. (2024). Low-cost bio-waste carbon nanocomposites for sustainable electrochemical devices: A systematic review. *Materials Today Communications*, 38: 108034. <https://doi.org/10.1016/j.mtcomm.2024.108034>
- [3] Hoffmann, M.M. (2022). Polyethylene glycol as a green chemical solvent. *Current Opinion in Colloid & Interface Science*, 57: 101537. <https://doi.org/10.1016/j.cocis.2021.101537>
- [4] Dhawan, S., Varma, M., Sinha, V.R. (2005). High molecular weight poly (ethylene oxide)-based drug delivery systems: Part I: Hydrogels and hydrophilic matrix systems. *Pharmaceutical Technology*, 29(5): 72-80.
- [5] Hu, D., Liu, W., Yu, W., Huang, L., Ji, C., Liu, X., Lu, Z. (2023). Psyllium seed husk regulates the gut microbiota and improves mucosal barrier injury in the colon to attenuate renal injury in 5/6 nephrectomy rats. *Renal Failure*, 45(1): 2197076. <https://doi.org/10.1080/0886022X.2023.2197076>
- [6] Agrawal, R. (2021). Psyllium: A source of dietary fiber. In *Dietary Fibers*. IntechOpen.
- [7] Singh, A., Benjakul, S., Prodpran, T., Nuthong, P. (2021). Effect of psyllium (*Plantago ovata* Forsk) husk on characteristics, rheological and textural properties of threadfin bream surimi gel. *Foods*, 10(6): 1181. <https://doi.org/10.3390/foods10061181>
- [8] Majmudar, H., Mourya, V., Devdhe, S., Chandak, R. (2013). Pharmaceutical applications of ispaghula husk: Mucilage. *International Journal of Pharmaceutical Sciences Review and Research*, 18(1): 49-55.
- [9] Waleed, M., Saeed, F., Afzaal, M., Niaz, B., et al. (2022). Structural and nutritional properties of psyllium husk arabinoxylans with special reference to their antioxidant potential. *International Journal of Food Properties*, 25(1): 2505-2513. <https://doi.org/10.1080/10942912.2022.2143522>
- [10] Al-Akhras, M.A., Telfah, M., Shakhathreh, M.N., Telfah, A., Mousa, M.S., Narayanaswamy, V., Obaidat, I.M. (2023). Optical and chemical investigations of PEO thin films incorporated with curcumin nanoparticle: Effect of film thickness. *Biointerface Research in Applied Chemistry*, 13(2): 143. <https://doi.org/10.33263/BRIAC132.143>
- [11] Telfah, A.D., Abdalla, S., Ferjani, H., Tavares, C.J., Etkorn, J. (2024). Optical, electrical, and structural properties of polyethylene oxide/fullerene nanocomposite films. *Physica B: Condensed Matter*, 679: 415787. <https://doi.org/10.1016/j.physb.2024.415787>
- [12] Abdali, K., Al-Bermany, E., Tuama, A.N. (2024). Unveiling the potential of elettaria cardamomum husk ash as feedstock nanofibers in improving the structure, optical, dielectric, and antibacterial performance of peo polymer for optoelectronic and biological applications. *Nano Biomed. Eng.*
- [13] Abdali, K. (2023). Novel flexible glass composite film for stretchable devices applications. *Silicon*, 15(12): 5187-5195. <https://doi.org/10.1007/s12633-023-02414-6>
- [14] Muheddin, D.Q., Aziz, S.B., Mohammed, P.A. (2023). Variation in the optical properties of PEO-based composites via a green metal complex: Macroscopic measurements to explain microscopic quantum transport from the valence band to the conduction band. *Polymers*, 15(3): 771. <https://doi.org/10.3390/polym15030771>
- [15] Yang, Z., Zhang, Y., Wen, B. (2019). Enhanced electromagnetic interference shielding capability in bamboo fiber@ polyaniline composites through microwave reflection cavity design. *Composites Science and Technology*, 178: 41-49. <https://doi.org/10.1016/j.compscitech.2019.04.023>
- [16] Al-Bermany, E., Mekhalif, A.T.M., Banimuslem, H.A., Abdali, K., Sabri, M.M. (2023). Effect of green synthesis bimetallic Ag@ SiO₂ core-shell nanoparticles on absorption behavior and electrical properties of PVA-PEO nanocomposites for optoelectronic applications.

- Silicon, 15(9): 4095-4107. <https://doi.org/10.1007/s12633-023-02332-7>
- [17] Čović, A., Stipanelov Vrandečić, N. (2021). Influence of poly (ethylene oxide) sample preparation on the results of thermogravimetric analysis. *ST-OPEN*, 2: e2021.1806.8. <https://doi.org/10.48188/so.2.5>
- [18] Gondaliya, N., Kanchan, D.K., Sharma, P., Joge, P. (2011). Structural and conductivity studies of poly (ethylene oxide)–silver triflate polymer electrolyte system. *Materials Sciences and Applications*, 2(11): 1639-1643. <https://doi.org/10.4236/msa.2011.211218>
- [19] Solaberrieta, I., Jiménez, A., Cacciotti, I., Garrigós, M.C. (2020). Encapsulation of bioactive compounds from aloe vera agrowastes in electrospun poly (ethylene oxide) nanofibers. *Polymers*, 12(6): 1323. <https://doi.org/10.3390/polym12061323>
- [20] Al-Shamari, A.A., Abdelghany, A.M., Alnattar, H., Oraby, A.H. (2021). Structural and optical properties of PEO/CMC polymer blend modified with gold nanoparticles synthesized by laser ablation in water. *Journal of Materials Research and Technology*, 12: 1597-1605. <https://doi.org/10.1016/j.jmrt.2021.03.050>
- [21] Goldstein, J.I., Newbury, D.E., Michael, J.R., Ritchie, N.W., Scott, J.H.J., Joy, D.C. (2017). *Scanning Electron Microscopy and X-Ray Microanalysis*. Springer.
- [22] Di Marco, G., Lanza, M., Pennisi, A., Simone, F. (2000). Solid state electrochromic device: behaviour of different salts on its performance. *Solid State Ionics*, 127(1-2): 23-29. [https://doi.org/10.1016/S0167-2738\(99\)00265-9](https://doi.org/10.1016/S0167-2738(99)00265-9)
- [23] Morán, D., Gutiérrez, G., Blanco-López, M.C., Marefati, A., Rayner, M., Matos, M. (2021). Synthesis of starch nanoparticles and their applications for bioactive compound encapsulation. *Applied Sciences*, 11(10): 4547. <https://doi.org/10.3390/app11104547>
- [24] Dularia, C., Sinhmar, A., Thory, R., Pathera, A.K., Nain, V. (2019). Development of starch nanoparticles based composite films from non-conventional source-Water chestnut (*Trapa bispinosa*). *International Journal of Biological Macromolecules*, 136: 1161-1168. <https://doi.org/10.1016/j.ijbiomac.2019.06.169>
- [25] Abdelrazek, E.M., Abdelghany, A.M., Badr, S.I., Morsi, M.A. (2016). Evaluation of optical parameters and structural variations of UV irradiated (PEO/PVP)/Au polymer nanocomposites. *Research Journal of Pharmaceutical, Biological and Chemical Sciences*, 7(2): 1877-1890.
- [26] Banerjee, M., Jain, A., Mukherjee, G.S. (2018). Spectroscopic evaluation of optical parameters of a transition metal salt filled polymer material. *Defence Science Journal*, 68(2): 225. <https://doi.org/10.14429/dsj.68.12331>
- [27] Hassouni, M.H., Mishjil, K.A., Chiad, S.S., Habubi, N.F. (2013). Effect of gamma irradiation on the optical properties of Mg doped CdO Thin films deposited by Spray Pyrolysis. *International Letters of Chemistry, Physics and Astronomy*, 11: 26-37.
- [28] Jabbar, S.A., Khalil, S.M., Abdulridha, A.R., Al-Bermany, E., Karar, A. (2022). Dielectric, AC Conductivity and Optical characterizations of (PVA-PEG) Doped SrO Hybrid nanocomposites. *Key Engineering Materials*, 936: 83-92. <https://doi.org/10.4028/p-41a757>
- [29] Sangawar, V., Golchha, M. (2013). Evolution of the optical properties of Polystyrene thin films filled with Zinc Oxide nanoparticles. *International Journal of Scientific & Engineering Research*, 4(6): 2700-2705.
- [30] Abdali, K., Al-Bermany, E., Abass, K.H. (2023). Impact the silver nanoparticles on properties of new fabricated polyvinyl alcohol-polyacrylamide-polyacrylic acid nanocomposites films for optoelectronics and radiation pollution applications. *Journal of Polymer Research*, 30(4): 138. <https://doi.org/10.1007/s10965-023-03514-y>
- [31] Al-Rubaye, S.A.J., Al-Isawi, N.A., Abdulridha, A.R. (2021). Preparation and study the electrical and optical properties for (PVA-PEG-Sr₂O₃) Nanocomposites. *Neuroquantology*, 19(10): 47-56.